THE JOURNAL OF PHYSICAL CHEMISTRY C
A JOURNAL OF THE AMERICAN CHEMICAL SOCIETY

pubs.acs.org/JPCC

Article

Dynamical Immiscibility of Aqueous Carbonate Fluid in the Shortite−Water System at High-Pressure−Temperature Conditions

Sergey V. Goryainov, Svetlana N. Krylova, Ulyana O. Borodina, and Alexander S. Krylov*

Cite This: *J. Phys. Chem. C* 2021, 125, 18501−18509

Read Online

ACCESS | Metrics & More | Article Recommendations | Supporting Information

ABSTRACT: Anhydrous carbonate shortite, $Na_2Ca_2(CO_3)_3$, compressed in water at high pressure−temperature (up to 5 GPa, 350 °C) was studied by Raman spectroscopy. At 3.2 GPa and 250 °C, shortite begins to dissolve, followed by crystallization of aragonite and aragonite'. The unusual behavior of aqueous carbonate fluid was observed at 4.8 GPa and 300−350 °C. This process is characterized by the active formation of microbubbles within 2−60 s that are inserted one into another. Microbubbles are considered to be a result of the two immiscible fluid stratification. This dynamical immiscibility of the fluid accompanies the appearance of several crystalline carbonates and organic molecular crystals. Na-formate and some polymorphs of Ca-formate were observed.

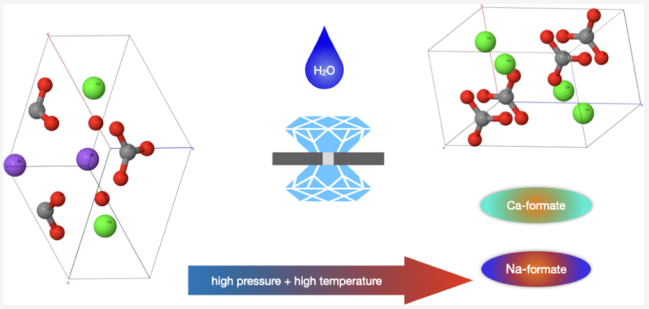

INTRODUCTION

Shortite $Na_2Ca_2(CO_3)_3$ is a rare carbonate mineral, which was first found in sedimentary rocks of Green River Basin, Wyoming.[1,2] The interest in shortite is mainly related to its occurrence within melt inclusions in deep-seated mantle mineral assemblages,[3,4] as well as kimberlite and carbonatite rocks. In particular, investigated shortite is a predominant phase of carbonate−chloride nodules found in kimberlites from Udachnaya east pipes.[5,6] These nodules consist of intercalated chloride and carbonate layers, the latter being composed of either shortite−northupite $Na_3Mg(CO_3)_2Cl$−calcite $CaCO_3$ assemblages or zoned aggregates of K-rich nyerereite $(Na(K))_2Ca(CO_3)_2$ in the core and shortite in the rim. The substance from which these nodules were formed is supposed to have the mantle origin, thus providing new insights into the composition and evolution of kimberlite melt, including the processes of diamond formation. The synthesized $Na_2Ca_2(CO_3)_3$ has perfect optical properties:[6,7] UV-transparent, and noncentrosymmetric $Na_2Ca_2(CO_3)_3$ has the 3 × KDP second-harmonic generation coefficient.

Recently, stability of $CaCO_3$ carbonate minerals (calcite, aragonite, vaterite,[8] and their polymorphs) and their Raman vibrational properties are actively investigated,[9−12] whereas Na−Ca carbonates are still less studied. $Na_2Ca_2(CO_3)_3$ crystallizes in space group *Amm*2 in the orthorhombic unit cell with parameters a = 4.9720(9) Å, b = 11.068(3) Å, and c = 7.1271(14) Å.[2] Amorphous calcium carbonate $CaCO_3$ is a precursor to crystalline phases in biomineral systems and one of the metastable states forming upon inorganic precipitation.[13] Isotropic and hydrous properties of amorphous carbonate allow biosystems to form complex compounds in the shells and skeletons. The restoration of synthesis conditions for bioorganic carbonate materials in which glassy carbonate often plays a precursor is prospective. The abiogenic origin of hydrocarbons in the core and mantle is discussed in the review paper.[14] Carbonate anions $(CO_3)^{2-}$ are considered as stable structural groups in carbonate minerals and fluids up to mantle conditions.[15,16] The formation of amorphous carbonate and its stability at high P−T conditions are still scantly studied. Shortite is unstable[17] at 3 GPa and above 800 °C in anhydrous medium ZrO_2.

Vennari's group studied shortite under high pressure−temperature (P−T) conditions.[18] The mentioned experiment does not correspond to the Earth's deep processes (i.e., do not correspond to geotherm). Also, the selected medium does not correspond to any natural environment, in which the rock was compressed under mantle conditions during its growth and subsequent exhumation (in the case of the joint formation of kimberlite diamonds and shortite).

In the first experiment, the methanol−ethanol mixture was chosen as the compressing medium. This medium does not occur in terrestrial conditions, while shortite was compressed to 26 GPa at room temperature. Their other experiment was dry compression of shortite at room temperature and a high pressure of 28 GPa. Then, they turned on laser heating of the sample to the estimated temperature in the range 1600−2000

Received: June 9, 2021
Revised: July 27, 2021
Published: August 18, 2021

Downloaded via STATE PUBLIC SCITECH LIBRARY SB RAS on November 8, 2021 at 07:04:12 (UTC).
See https://pubs.acs.org/sharingguidelines for options on how to legitimately share published articles.

© 2021 American Chemical Society

https://doi.org/10.1021/acs.jpcc.1c05077
J. Phys. Chem. C 2021, 125, 18501−18509

°C. The second experiment of this group[18] also does not correspond to earthly processes.

The most typical medium for the combined synthesis of kimberlite diamond[19,20] and shortite is a fluid with a variable (from low to high) water content. Another natural process is the diving of the oceanic slab, containing carbonate-rich rock and a large amount of water, into subduction zones. In this regard, we chose water as the pressure-transmitting medium. We decided the $P-T$ trend, which is located near the geotherm, which corresponds to the modeling of processes under terrestrial conditions in the mantle depths. The previous experiment does not correspond to the Earth's deep processes (i.e., do not correspond to the geotherm).[18] As shown in our experiments, this environment plays a crucial role in determining the stability and decomposition of this carbonate.

The present work aims to investigate stability and possible transformations of shortite compressed in water medium at $P-T$ parameters of 0−5 GPa, 20−350 °C, using in situ and ex situ Raman spectroscopy. Possible transformations may include reversible and irreversible polymorphism, amorphization, the formation of the hydrated phase, and decomposition of shortite. The in situ method allows control of the actual state of aqueous C−O−H fluid that is still scantly investigated. For instance, authors[21] studied CO_2-H_2O fluid at high $P-T$ and revealed the surprising effect: formation of solid H_2CO_3. Along the way, we also focus on the behavior of aqueous Ca−Na−carbonate fluid under high $P-T$ conditions.

EXPERIMENT

The Raman spectra were obtained using an Ar^+ laser with a wavelength of 514.5 nm and recorded on a HORIBA Jobin Yvon T64000 triple spectrometer. The incident beam power on the sample was 5 mW. The spectra were recorded in the range from 10 to 4000 cm^{-1} with a spectral resolution of 2 cm^{-1}, pixel coverage 0.3 cm^{-1}. Raman scattering of processes occurring in shortite samples at high hydrostatic pressures and temperatures was carried out using a restively heated cell with diamond anvils (DAC) with Diacell μScopeDAC-HT(G) membrane-type anvils purchased from EasyLab (UK).[22−25] The cell had a water-cooled casing. During measurements, the anvils were blown with an inert argon flow with a 1 percent admixture of hydrogen. In the experimental arrangement, stainless steel gasket, initially 250 μm thick, was used. The gasket, squeezed at its periphery to a thickness of 80 μm, had a 150 μm hole prepared using a spark discharge. The pressure in the cell was determined using photoluminescence data (lines R1 and R2) of the ruby. The accuracy of the determination of P was 0.05 GPa. Temperature calibration (dependence of sample temperature on thermocouple temperature; the latter was determined with an accuracy of 0.05 °C) was performed by the method in refs 26 and 27. The accuracy of this method for determining the temperature of a sample is estimated as 5 °C.

As part of the study, two experiments were conducted with different $P-T$ parameters, which are shown in Figure 1. The experimental points were compared with the $P-T$-diagram of the stability of aragonite and calcite.[28] The sample of polycrystalline shortite was taken from Udachnaya East Kimberlites (Russia). The chemical composition $Na_{1.94}Ca_{2.02}Sr_{0.01}K_{0.01}(CO_3)_3$ is close to idealized shortite formula $Na_2Ca_2(CO_3)_3$.[29]

The ex situ experiment was performed later. The samples participating in the in situ research with high pressures and temperatures were studied by Raman spectroscopy in the air at atmospheric pressure. In the ex situ study, we used the HORIBA Jobin Yvon HR800 spectrometer with excitation by a laser line of 532 nm wavelength.

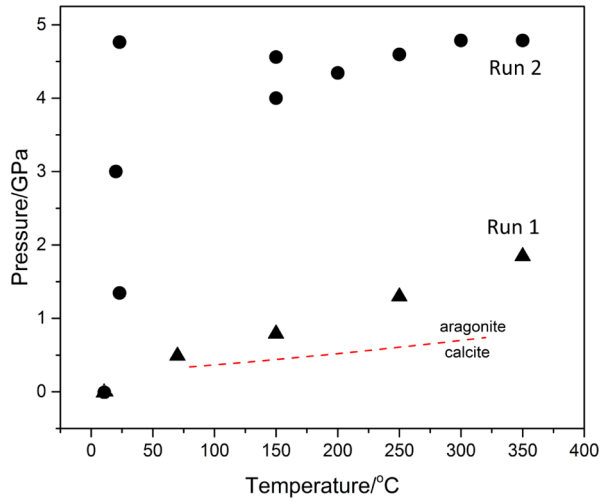

Figure 1. $P-T$ parameters of two in situ experiments (run 1 and run 2). The dashed line corresponds to the aragonite−calcite transition.

The PeakFit program package was used for the deconvolution of Raman spectra into Voigt amplitude functions.[30]

Lattice-dynamical calculations of vibrational spectra were successfully used for many structures.[22,23,31−33] In our work, the theoretical calculations for the shortite were carried out by the plane-wave pseudopotential method based on density functional theory using the Cambridge serial total energy package (CASTEP) code.[34] Pseudoatom calculations are performed for C: 2s2, 2p2; O: 2s2, 2p4; Na: 2s2, 2p6, 3s1; Ca: 3s2, 3p6, 4s2. The structures were relaxed using the Broyden, Fletcher, Goldfarb, and Shannon minimization method algorithm. The lattice constants and atom coordinates were optimized by minimizing the total energy. Through a series of convergence studies concerning cutoff energies and k-points, the cutoff energies were set to 660 eV, and the K-space integration over the Brillouin zone was carried out using a 4 × 4 × 5 k-point Monkhorst−Pack mesh.[35] The parameters were tested to ensure that the self-consistent total energies converged to within 5.0×10^{-8} eV/atom.

RESULTS AND DISCUSSION

In Situ Raman Study. $Na_2Ca_2(CO_3)_3$ belongs to the orthorhombic space group $Amm2$ (N 38 in crystallographic tables) at atmospheric conditions.[2,6,18] Raman, infrared, and acoustic mode representations of the Brillouin zone center are as follows

$$\Gamma_{\text{Raman}} = 14A_1 + 7A_2 + 10B_1 + 14B_2 \quad (1)$$

$$\Gamma_{\text{IR}} = 14A_1 + 10B_1 + 14B_2 \quad (2)$$

$$\Gamma_{ac} = A_1 + B_1 + B_2 \quad (3)$$

Here A_1 and A_2 are nondegenerate symmetric irreducible representations. B_1 and B_2 are nondegenerate antisymmetric irreducible representations.

The nonempirical functionals local-density approximation and generalized gradient approximation (GGA) use only general rules of quantum mechanics and special limiting conditions to determine the parameters in a general form. Such

https://doi.org/10.1021/acs.jpcc.1c05077
J. Phys. Chem. C 2021, 125, 18501−18509

approximate functionals satisfy as many exact conditions as possible. We used the Perdew–Burke–Ernzerhof exchange–correlation functional for solids (PBEsol, GGA functional). The functional PBEsol (GGA) has been developed specifically to improve the description of exchange in solids, resulting in better structures and energetics for densely packed solids and their surfaces.[36] We have made the structural relaxation and optimization with the approximations to determine the lattice parameters (Table 1). The experimental and theoretical lattice parameters are in good agreement. The calculated Raman and infrared active modes for $Na_2Ca_2(CO_3)_3$ are presented in Supporting Information (Table S1).

Table 1. Lattice Parameters in the *Amm*2 Phase of $Na_2Ca_2(CO_3)_3$

	PBE sol (this work)	Exper.[2]
a (Å)	6.583919	6.561796
b (Å)	6.583919	6.561796
c (Å)	4.957725	4.947000
α (deg)	90	90
α (deg)	90	90
α (deg)	114.547308	114.412028

We compared the calculated spectra with the experimental one (Figure 2). The strongest modes at 1072 and 1091 cm^{-1} correspond to two components of symmetric stretching vibrations ν_{1L} (CO_3) and ν_1H (CO_2) (notation given for the nyererite spectrum[37]), which is consistent with the works.[18,29] Frost and Dickfos in their work[38] suggested that the strong bands at 1072 and 1091 cm^{-1} are assigned to CO_3 symmetric stretching. Our calculation makes it possible to clarify that only the 1072 cm^{-1} band corresponds to the CO_3 symmetric stretching. The other band at 1091 cm^{-1} corresponds to CO_2 stretching. The modes in the range 696–731 cm^{-1} belong to the split $(CO_3)^{2-}$ ν_4 mode of deformation vibrations. In the low-frequency region of the spectrum, 100–200 cm^{-1}, several modes are observed related to crystal lattice vibrations. The calculated vibration forms of the 1072 and 1091 cm^{-1} bands of shortite are presented in Figure S1.

The Raman spectra of the shortite at high *P*–*T* parameters are presented in Figure 3. The gradual broadening of the modes is observed with increasing pressure to 4.5 GPa and a further increase in temperature to 200 °C. The additional peak at 1100 cm^{-1} appears at 4.6 GPa, 250 °C. The change of the crystal shape and a decrease in the size observed visually under a microscope indicates the beginning of the dissolution of shortite in an aqueous medium at 4.6 GPa, 250 °C. The subsequent Raman spectra have a shape different from the spectrum at the initial parameters (the joining of the ν_1L CO_3 and ν_1H CO_3 modes). A new satellite peak at 1070 cm^{-1} appears with a decrease in pressure and temperature to 3.0 GPa, 20 °C. A new intermediate phase crystallizes from the solution. The intermediate phase is observed up to 4.8 GPa, 350 °C. With a subsequent pressure and temperature decreasing to 3.0 GPa, 20 °C, a new phase marked as aragonite' crystallizes from the solution. We consider that the intermediate HP–HT phase aragonite'. Their spectra of aragonite and aragonite' in the C–O stretching range are similar, and only one weak satellite peak at 1066–1070 cm^{-1} appears upon cooling. Their low-frequency spectra are weak and cannot be used for discernment.

The values of wavenumber and bandwidth for $(CO_3)^{2-}$ stretching modes of shortite at different *P*–*T* parameters are presented in Table 2.At the onset of the heating and the increase of pressure, the aqueous solution is saturated by dissolved carbonate ions ($(CO_3)^{2-}$, Na^+, and Ca^{2+}), it being homogeneous. At high *P*–*T* (4.8 GPa, 300–350 °C), we observed unusual behavior of the medium when aqueous carbonate fluid disintegrates into at least two components (Figure 4). This process is characterized by the active formation of microbubbles. Figure 4 (see also the video file

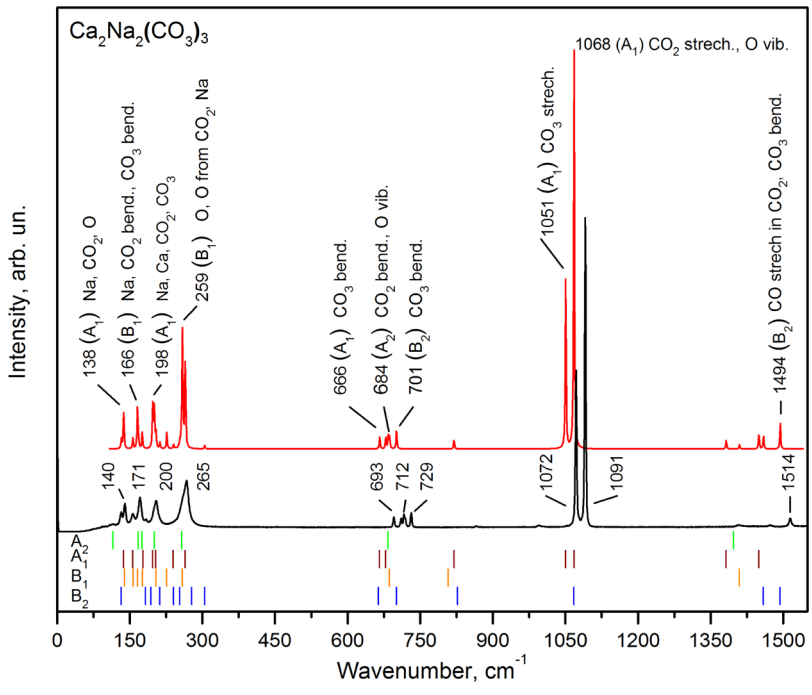

Figure 2. Experimental (in black) and calculated (color) Raman spectra of shortite.

https://doi.org/10.1021/acs.jpcc.1c05077
J. Phys. Chem. C 2021, 125, 18501–18509

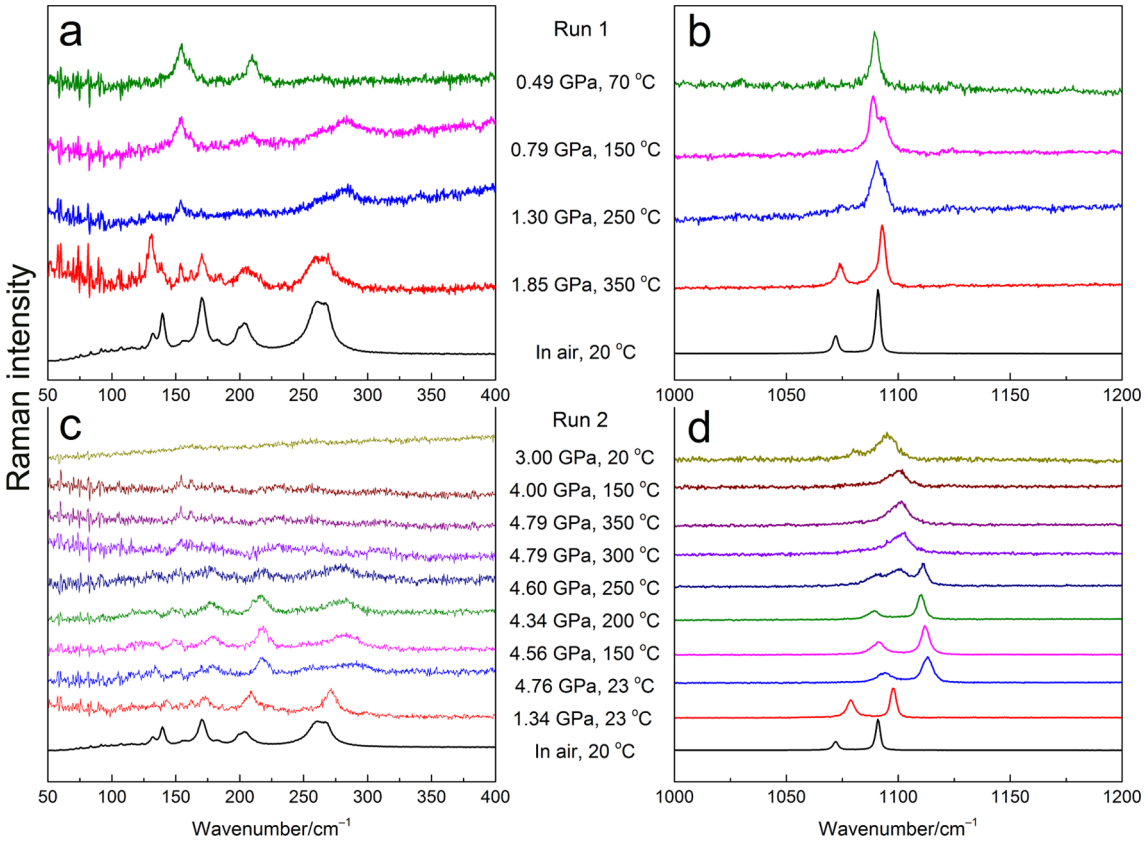

Figure 3. In situ shortite Raman spectra in the two regions: (a,c) from 50 to 400 cm^{-1} and (b,d) from 1000 to 1200 cm^{-1} at different $P-T$ parameters followed in the experimental order, starting from ambient conditions in air at 20 °C.

Table 2. Shortite Band Wavenumber and Bandwidth Values for Experimental $P-T$ Parameters

T, °C	P, GPa	ν_{1L}, cm^{-1}	ν_{1ad}, cm^{-1}	ν_{1H}, cm^{-1}	$FWHM_{1L}$, cm^{-1}	$FWHM_{1ad}$, cm^{-1}	$FWHM_{1H}$, cm^{-1}
			Atmospheric Condition				
23	0	1072		1091	2.4		2.15
			Run 1				
70	0.49	1074		1093	4.8		2.7
150	0.89	1074		1093	4.9		3.2
250	1.30	1087		1093	3.7		3.9
350	1.85	1088			4.3		
			Run 2				
23	1.34	1079		1098	4.4		4.2
23	4.76	1094		1113	7.9		7.9
150	4.56	1091		1112	6.9		4.3
200	4.34	1089		1110	8.1		3.9
250	4.60	1090	1100	1111	6.2	10.9	4.8
300	4.79	1096	1102			14.9	8.3
350	4.79	1095	1100			10.4	8.4
150	4.00	1096	1101			9.1	7.4
20	3.00	1081	1095			9.9	10.9

in Supporting Information) exhibits the dynamical formation of microbubbles. The single microbubbles and groups (equal or above 2), when one is inserted into another, formed the Russian nesting doll. The time of existence of each microbubble is often varied within 2−60 s or longer. Finishing the existence, it bursts or merges with other microbubbles.

At preparation of the set in the DAC, small bubbles with air (N_2 and O_2 gases are major components) were observed between shortite blocks and the metal surface of the gasket; then, the bubbles collapsed at the beginning compression (at P about 0.1 GPa).The observed microbubbles differ from usual bubbles mentioned and are considered to be the result of the stratification of two immiscible media: supercritical fluid (liquid−gas CO_2) and subcritical water fluid. Microbubbles in the fluid appeared during both HP−HT shortite−water experiments (run 1 and run 2 in Figure 1), starting from 250 °C.

Analysis of Chemical Reactions in Aqueous Carbonate Fluid. According to the first hypothesis, the formation of microbubbles in fluid occurs due to the stratification of two

https://doi.org/10.1021/acs.jpcc.1c05077
J. Phys. Chem. C 2021, 125, 18501−18509

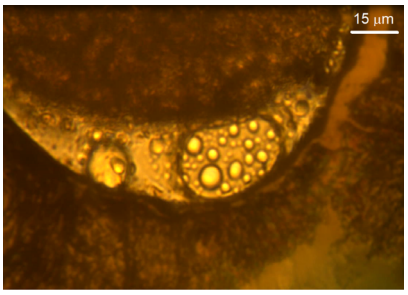

Figure 4. Microphotograph of the sample (dark part) and medium (transparent part) during shortite−water experiments at 4.8 GPa and 350 °C (run 2).

immiscible liquids: Na (monocationic) and Na−Ca (bicationic) carbonate aqueous solutions, whereas the Ca cation part of carbonate fluid precipitates into calcite, aragonite, and other polymorphs according to our HP−HT experiments. Shortite crystals dissolve in water and generate the fluid with the composition that is close to the subsolids, when the melting temperature is decreased. Hypothetically, one component of the immiscible solution may be considered as aqueous Na−Ca bicationic carbonate solution. Such a model of the medium with two liquids may in draft describe the solution stratification. This dynamical immiscibility of polycationic carbonate fluid has effects on the formation of carbonate phases, promoting the appearance of various carbonates and X-phases with organic molecules.

We assume that the following chemical reactions occur under pressure

$$(Na_2Ca_2CO_3)_3 + H_2O + CO_2 = 2(CaCO_3) + 2(HCOONa) + O_2 \quad (4)$$

$$CaCO_3 + H_2O + CO_2 = Ca(HCOO)_2 + O_2 \quad (5)$$

These reactions require excess CO_2, which is absent in the initial mixture—the shortite−water system. With heating (the more active the metal, the higher the required temperature), the carbonates decompose into oxides and carbon dioxide CO_2:

(1000 °C at atmospheric pressure)

$$Na_2CO_3 = Na_2O + CO_2 \quad (6)$$

(800 °C at atmospheric pressure)

$$CaCO_3 = CaO + CO_2 \quad (7)$$

These two reactions are unlikely. When carbonate interacts with water, bicarbonate is formed as the main product of carbonate hydrolysis

$$Na_2CO_3 + H_2O = NaHCO_3 + NaOH \quad (8)$$

The decomposition temperature of the carbonate ion is significantly lower in the case of using hydrocarbons. When heated, hydrocarbons transform into carbonates with the release of CO_2 and water.

(more or equal 100 °C at atmospheric pressure)

$$2(NaHCO_3) = Na_2CO_3 + CO_2 + H_2O \quad (9)$$

This reaction is probably realized in our shortite−water system when it is heated above 100 °C.

According to the second hypothesis, the immiscible aqueous fluid is composed of Na−Ca carbonate and organic molecular solutions, including possible liquid Na-formate. Note that the Na-formate melting temperature in air conditions is 253 °C. Upon further heating, it decomposes before boiling. Solid Ca-formate decomposes at 300 °C (before the melting). Unfortunately, data about the stability of these formates at high pressure are not available.

Carbonate decomposition and formation of organic crystals can pass through several stages, involving numerous reactions and producing additional products, including gas O_2, oxides, and hypothetical peroxides (Na_2O_2 and CaO_2) due to the possible presence of the excess molecules of O_2 in aqueous fluid. The last gas component is produced by noted reactions 4 and 5. Instead, this dissolved O_2, oxides, and peroxides play a secondary role because chemical reactions 6 and 7 are strongly suppressed at a moderate temperature of 350 °C used in experiments.

According to the third hypothesis, there is a stratification of the simple gas−liquid CO_2−H_2O system. The component CO_2 is in the supercritical state under P−T conditions above critical values, T_c = 31 °C and P_c = 7.4 MPa (73 bar).[39] The component H_2O is in the usual (subcritical) liquid state when the P−T parameters are lower critical values, T_c = 374 °C and P_c = 22 MPa (218 bar), that correspond to our conditions due to lower temperature. According to a work,[39] there is the gap in miscibility of CO_2−H_2O at least at moderate pressure. Accepting this plausible hypothesis, the stratification of the fluid in the shortite−water system, accompanied by unusual dynamical behavior of microbubbles, probably corresponds to immiscible two-component medium: supercritical fluid (CO_2 major component) and subcritical aqueous fluid (H_2O major component).

Ex Situ Raman Study. After two experiments at high P−T parameters, shortite samples were investigated in the air. The obtained ex situ Raman spectra confirmed the formation of a new phase, namely, aragonite (Figure S2), compared with aragonite spectra (RRUFF R080142). Furthermore, the possibility of aragonite formation with experimental parameters is also confirmed by the aragonite−calcite transition.

We did not register anhydrous carbonate Na_2CO_3 or its hydrated forms: sodium bicarbonate $NaHCO_3$, throne $Na_2CO_3{\cdot}NaHCO_3{\cdot}2H_2O$, $Na_2CO_3{\cdot}nH_2O$, and others. Note that $Na_2CO_3{\cdot}H_2O$ monohydrate is stable at temperatures above 35 °C at a pressure of 1 bar. The repeated action of probable chemical reactions (Supporting Information) leads to the consumption of Na_2CO_3 carbonate, as a result of which it does not precipitate in the crystalline or amorphous form as well as in the form of hydrated phases. This behavior explains our data from the Raman spectra analysis of the samples, which indicate the absence of Na-carbonates.

The Raman spectra of various substances produced in the ex situ experiment are presented in Figure 5. The ex situ Raman microprobe of the treated sample revealed different parts, where some phases were dominant, including the layer with conserved the shortite phase. This layer exhibits the Raman spectrum (2), close to the initial shortite spectrum (1). At this band, wavenumbers almost coincide within the accuracy of the measurement. This thin layer that lies on the bottom anvil surface during the experiment was the unsolved part of the shortite sample. This layer did not crack, which proves the lack of considerable mechanical stresses at high P−T conditions. Raman data and visual observation prove that shortite retained its crystalline structure and symmetry and did not undergo polymorphic transitions and hydration. It should be noted that

https://doi.org/10.1021/acs.jpcc.1c05077
J. Phys. Chem. C 2021, 125, 18501−18509

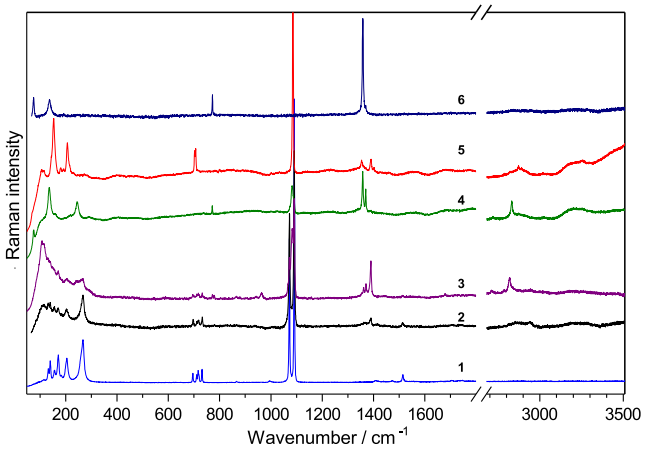

Figure 5. Ex situ Raman spectra of the shortite sample after high $P-T$ run 2 (2–6), compared with initial shortite (1) selected for the DAC experiment and recorded in air conditions. Different parts of the sample show the following phase composition: (2) shortite + X2; (3) aragonite' + shortite + X2; (4) aragonite' + X1; (5) aragonite + X2; (6) X1. The denotations used are as follows X1 and X2 are X1- and X2-phases, correspondingly; Arag is aragonite; Arag' is the comma phase of aragonite.

there are distinguishable differences in spectra of treated and initial shortite: bands additionally widen to 1.5–2 cm^{-1} and a low-wavenumber wing appears in the range of 80–200 cm^{-1} in the ex situ spectrum of the treated sample. The in situ Raman spectra (Figure 3) showed the transformation shortite into the third high-pressure phase, denoted here as aragonite' (comma phase). This phase is presented in Figure 5 (spectra 3 and 4). The Raman spectrum of aragonite' observed in the experiment (run 2) is similar to true aragonite observed in the experiment (run 1) by the main C–O stretching band at about 1083 cm^{-1} but differs in the low-wavenumber range. The major part of the transformation in the run 2 sample contains this aragonite' and unknown phases (X1 and X2). Spectrum (4) exhibits the presence of aragonite' and the X1-phase. Spectrum (3) in Figure 5 exhibits the existence of shortite, aragonite' and the X2-phase. The Raman spectra of shortite and other carbonates are included in Table S4. The first line gives numbers (1–6), which corresponded to the number of the spectrum in Figure 5, and number (7) is a low spectrum in Figure S2 (aragonite), with others being (8) Na-formate, (9) α-Ca-formate, and (10) interpretation of Raman modes. The second line explains the phase composition; the third line presents the file name of the spectrum. Remarks and denotation: X1 and X2 are X1 and X2-

Table 3. Raman Spectra of Shortite and Other Carbonates Produced upon HPT Treatment (Band Wavenumbers in cm^{-1})

1 In. Sh.	2 Sh. + X2	3 Ar.' + Sh. + X2	4 Ar.' + X1	5 Ar. + X2	6 X1	7 Ar.	8 Na form.	9 α-Ca form.	10 Interp.
	113	24							(CO_3) lib., (CO_2) bend.
132	132	131							(CO_2) bend.
140	140	139							Na, (CO_2) bend., O vib.
156	156								(CO_3) trans.
171	170	170							Na, (CO_2) bend., (CO_3) bend.
200	204	204							Na, Ca, (CO_2) and (CO_3) as whole
260									(CO_3) libr.
265	267	265							(O) vib., O from (CO_2), Na vib.
693	696	696							bend. (CO_3)
712	712	712							bend. O–C–O, O vib.
718	718	717							bend. O–C–O
729	732	732							bend. (CO_3)
996		964							impurity SO_4
1072	1072	1072							sym.str. CO_3
1091	1091	1091							sym.str. O–C–O, O vib.
1514	1514	1514							str. C–O in (CO_2), (CO_3) bend.
		Arag':	Arag':	Arag:		Arag:			
		111	110	106, 115		112			
			160	153		153, 179			
		242	245	207	245	206	248/245		NaHCOO rot.[41] (a-ax.)
				703, 707		702, 707			
		1066							sym.str. C–O
		1083	1083	1086		1085			sym.str. C–O
		1089	1089						sym.str. C–O
						1461			asym.str. C–O
	X2:	X2:	X1:	X2:					
			76		75		/74		NaHCOO transl.[41]
			136		137		/135		NaHCOO rot.[41] (c-ax.)
		772.8	771.4		772		772/770	790	bend. O–C–O
		1354	1358	1353	1358		1359/1355	1352	sym.str. C–O
	1364	1362						1361	sym.str. C–O
			1370		1369		1369/		sym.str. C–O
	1389	1390		1390				1380, 1420	sym.str. C–O
		2819	2832	2872			2830/2830		str. C–H
				2892				2897	str. O–H

https://doi.org/10.1021/acs.jpcc.1c05077
J. Phys. Chem. C 2021, 125, 18501–18509

phases, correspondingly; Arag is aragonite; Arag' is the comma phase of aragonite.

The main C−O stretching band at 1083 cm^{-1} of observed aragonite' is very close to that of calcite at 1086(5) cm^{-1} (major polymorph no. 1 of $CaCO_3$ according to work[8]) and aragonite at 1085 cm^{-1} (major $CaCO_3$ polymorph N 2). This peak of aragonite' differs from that of vaterite (major $CaCO_3$ polymorph[8] N 3, having the strongest band at 1090 cm^{-1} and its shoulder at 1075 cm^{-1}; moreover, the last two bands are considerably wider. The first aragonite' lattice band at 111 cm^{-1} is very close to the aragonite doublet (106 and 115 cm^{-1}). The second one (160−170 cm^{-1}) slightly shifted from the aragonite band (153 cm^{-1}) and calcite band (155 cm^{-1}). Another lattice band at 242−245 cm^{-1} remarkably differs from that of aragonite (207 cm^{-1}) and calcite (282 cm^{-1}). Besides, the main C−O stretching band of aragonite' has the form of a doublet, with the dominant one at 1083 cm^{-1} and the shoulder at 1089 cm^{-1}. Taking similarity with the aragonite spectrum into account, we named this phase as aragonite'. The Raman data (Figure 5) and $P-T$ plot of the experiment (run 2) allow us to suggest that aragonite' is possibly the aragonite-III polymorph studied in the work.[9]

The Raman spectrum of the X1-phase (low-wavenumber bands) has two strong bands at 75 and 135−137 cm^{-1} in Figure 5 (spectra 4 and 6). The intensity of the band at 75 cm^{-1} considerably decreased because of device absorption in low wavenumbers due to the edge optical filter. The Raman spectrum of the X1-phase has characteristic bands at 772, 1357−1358, and 1369−1370 cm^{-1} (the second is the most strong) as much as the set in the C−H stretching range at 2831 and 2872 cm^{-1}, where the first band is more strong. The Raman spectrum of the X2-phase exhibits characteristic bands at 772, 779 (weak doublet), 1354, 1362, 1371, and 1390 cm^{-1} (the second is the most intense) as much the C−H stretching bands at 2712 and 2819 cm^{-1}, where the last one is more strong (Figure 5). The Raman spectra of shortite and other carbonates are included in Table 3. The first line gives numbers (1−6) corresponding to the number of the spectrum in Figure, and number (7) is the low spectrum in Figure S2 (aragonite), (8) Na-formate, (9) α-Ca-formate, (10) interpretation of Raman modes. The second line explains the phase composition; the third line presents the file name of the spectrum. Remarks and denotation: X1 and X2 are X1 and X2-phases, correspondingly; Arag is aragonite; Arag' is the comma phase of aragonite. Table S4 includes the Raman spectra of shortite and other carbonates formed during HPT treatment during cycle 1 (1, 2, and 5−7 columns) and cycle 2 (3 and 4 columns). The data in columns 1−7 were obtained in this work. The data of column 8 are from other sources.[40−42] The data of column 9 are taken from another article.[43] Our interpretation of the spectra is presented in column 10; it includes some descriptions of vibrational modes presented in other articles.[41,42]

The Raman spectra of X1- and X2-phases are very similar (concerning the number of bands and their intensity) to that of the linear 3-atomic molecule. The list of candidates for such molecule includes: formic acid, dioxirane H_2CO_2, methanediol $H_2C(OH)_2$, formaldehyde $H_2C(OH)_2$, 1,4-dioxane HCOOH, and formate. Among these candidates, Na-formate is considered most believable. No distinct Raman bands in the O−H stretching range were detected, albeit they could be presented as weak wide bands covered by average luminescence that is increased to 3600 cm^{-1}. The Raman spectrum of the X1-phase is very close to that of anhydrous Na-formate.[41,42,44−46] The Raman spectrum of the X2-phase is close to the α-Ca-formate.[43] Thus, Na-formate and Ca-formate polymorphs are possible products of carbonate decomposition in water medium at high $P-T$.

CONCLUSIONS

Combining in situ and ex situ Raman microspectroscopic methods provides more detailed information about changes in samples and fluid that occurred at high pressure and high temperature. The theoretical analysis (CASTEP) of the phonon spectra of a shortite crystal cell made it possible to interpret the observed Raman bands. It was found that at parameters 4.6 GPa and 250 °C, shortite begins to dissolve in the water medium. Upon further increasing the parameters, new carbonate phases (aragonite type) form, that is, in situ observed up to the studied 4.8 GPa and 350 °C.

All transformations observed in the shortite−water system are supported with a fluid, passing through the stage of dissolution of carbonate in the fluid. The formation of new phases (carbonates of aragonite and aragonite', the crystals X1 and X2) took place in the fluid. At the same time, these carbonates arose directly in the zone where the original shortite crystal had been previously placed, while the microcrystallites of the X1 and X2 phases, which are certainly Na- and Ca-formates, respectively, grew mainly in the area, where microbubbles in the fluid were previously observed. These phases X1 and X2 in a lower concentration were also ex situ found in all regions of the transformation products obtained during the HP−HT experiment.

The peculiar behavior of the aqueous carbonate fluid was observed under high $P-T$ conditions, which is significantly different from the usual decomposition of carbonates, with the release of CO_2 gas bubbles when only the enlargement of gas bubbles and the bubble fusion occurs. The fluid stratification observed in the shortite-water system and the dynamic complex behavior of microbubbles (appearance, growth, their movement, the formation of the superstructure as microbubbles inserted into each other, their coalescence, and collapse) probably corresponds to the special behavior of two immiscible media: supercritical fluid (liquid−gas CO_2) and subcritical water fluid. Additionally, it is possible that a more complex mechanism of dynamic separation of the fluid into a carbonate solution and a formate melt is involved.

A recent work[47] showed the presence of a wide variety of organic molecules in a number of minerals (olivine, garnet, the diamond in the form of inclusions); however, no formates were found. In our study, the first stage of the conversion of the inorganic matter (carbonates) to the salts of organic acids that was missing was observed. Shortite, being a participant in transformations in kimberlites, when immersed in aqueous fluid at high $P-T$ (up to 5 GPa, 350 °C), undergoes a stage of partial transformation into other carbonates (aragonite type) and, in addition to this, the simultaneous decomposition of carbonate ions $(CO_3)^{2-}$, which gives rise to the first organic molecules, which are formates, from inorganic matter. It is likely that under upper mantle conditions, these formates at higher $P-T$ parameters can be transformed into other more complex organic compounds, some of which are likely to arise simultaneously with the appearance of diamond crystallites.[19,20]

The oceanic slab can contain significant amounts of carbonates in the form of bottom sediments, which sink into

https://doi.org/10.1021/acs.jpcc.1c05077
J. Phys. Chem. C 2021, 125, 18501−18509

subduction zones in the upper mantle depths. According to our investigation, when immersed and heated (up to 100−350 °C), these carbonates can partially decompose, forming fluids, precipitating to the sodium and the calcium salts of formic acid. Thus, even in a small 1−2 percent conversion of carbonates into organic matter (that is underestimated), this mechanism can be the major (in terms of tonnage) source of abiogenic synthesis of organic matter in the upper mantle layers of the Earth.

■ ASSOCIATED CONTENT

Supporting Information

The Supporting Information is available free of charge at https://pubs.acs.org/doi/10.1021/acs.jpcc.1c05077.

Experiment and calculation (PDF)

In situ microbubble formation (MP4)

■ AUTHOR INFORMATION

Corresponding Author

Alexander S. Krylov − *Kirensky Institute of Physics, Federal Research Center KSC SB RAS, 660036 Krasnoyarsk, Russia;* orcid.org/0000-0001-8949-0584; Email: shusy@iph.krasn.ru

Authors

Sergey V. Goryainov − *Sobolev Institute of Geology and Mineralogy SB RAS, 630090 Novosibirsk, Russia*

Svetlana N. Krylova − *Kirensky Institute of Physics, Federal Research Center KSC SB RAS, 660036 Krasnoyarsk, Russia;* orcid.org/0000-0003-1277-6044

Ulyana O. Borodina − *Sobolev Institute of Geology and Mineralogy SB RAS, 630090 Novosibirsk, Russia*

Complete contact information is available at: https://pubs.acs.org/10.1021/acs.jpcc.1c05077

Notes

The authors declare no competing financial interest.

■ ACKNOWLEDGMENTS

The reported study was funded by the RFBR and DFG, project number 21-52-12018. Work is done on the state assignment of the Sobolev Institute of Geology and Mineralogy, Kirensky Institute of Physics SB RAS, Equipment of Federal Research Center of Krasnoyarsk Science Center SB RAS, and supported by the Ministry of Science and Higher Education. Authors thank A.N. Vtyurin, A.G. Sokol, A.Yu. Likhacheva, and A.F. Shatskiy for fruitful discussion.

■ REFERENCES

(1) Fahey, J. J. Shortite, a new carbonate of sodium and calcium. *Am. Mineral.* **1939**, *24*, 514−518.

(2) Dickens, B.; Hyman, A.; Brown, W. E. Crystal structure of $Ca_2Na_2(CO_3)_3$ (shortite). *J. Res. Natl. Bur. Stand. A Phys. Chem.* **1971**, *75*, 129−135.

(3) Golovin, A. V.; Sharygin, I. S.; Korsakov, A. V. Origin of alkaline carbonates in kimberlites of the Siberian craton: Evidence from melt inclusions in mantle olivine of the Udachnaya-East pipe. *Chem. Geol.* **2017**, *455*, 357−375.

(4) Golovin, A. V.; Sharygin, I. S.; Kamenetsky, V. S.; Korsakov, A. V.; Yaxley, G. M. Alkali-carbonate melts from the base of cratonic lithospheric mantle: links to kimberlites. *Chem. Geol.* **2018**, *483*, 261−274.

(5) Kamenetsky, V. S.; Sharygin, V. V.; Kamenetsky, M. B.; Golovin, A. V. Chloride-carbonate nodules in kimberlites from the Udachnaya pipe: alternative approach to the evolution of kimberlite magmas. *Geochem. Int.* **2006**, *44*, 935−940.

(6) Song, Y.; Luo, M.; Zhao, D.; Peng, G.; Lin, C.; Ye, N. Explorations of new UV nonlinear optical materials in the Na_2CO_3−$CaCO_3$ system. *J. Mater. Chem. C* **2017**, *5*, 8758−8764.

(7) Rashchenko, S. V.; Bakakin, V. V.; Shatskiy, A. F.; Gavryushkin, P. N.; Seryotkin, Y. V.; Litasov, K. D. Noncentrosymmetric Na2Ca4(CO3)5 Carbonate of "M13M23XY3Z" Structural Type and Affinity between Borate and Carbonate Structures for Design of New Optical Materials. *Cryst. Growth Des.* **2017**, *17*, 6079−6084.

(8) Nehrke, G.; Poigner, H.; Wilhelms-Dick, D.; Brey, T.; Abele, D. Coexistence of three calcium carbonate polymorphs in the shell of the Antarctic clamLaternula elliptica. *Geochem., Geophys., Geosyst.* **2012**, *13*, Q05014.

(9) Bayarjargal, L.; Fruhner, C.-J.; Schrodt, N.; Winkler, B. $CaCO_3$ phase diagram studied with Raman spectroscopy at pressures up to 50 GPa and high temperatures and DFT modeling. *Phys. Earth Planet. Inter.* **2018**, *281*, 31−45.

(10) Gavryushkin, P. N.; Martirosyan, N. S.; Inerbaev, T. M.; Popov, Z. I.; Rashchenko, S. V.; Likhacheva, A. Y.; Lobanov, S. S.; Goncharov, A. F.; Prakapenka, V. B.; Litasov, K. D. Aragonite-II and $CaCO_3$-VII: new high-pressure, high-temperature polymorphs of $CaCO_3$. *Cryst. Growth Des.* **2017**, *17*, 6291−6296.

(11) Gillet, P.; Biellmann, C.; Reynard, B.; McMillan, P. Raman spectroscopic studies of carbonates. Part I: high-pressure and high-temperature behaviour of calcite, magnesite, dolomite and aragonite. *Phys. Chem. Miner.* **1993**, *20*, 1−18.

(12) Litasov, K. D.; Shatskiy, A.; Gavryushkin, P. N.; Bekhtenova, A. E.; Dorogokupets, P. I.; Danilov, B. S.; Higo, Y.; Akilbekov, A. T.; Inerbaev, T. M. P-V-T equation of state of $CaCO_3$ aragonite to 29 GPa and 1673 K: In situ X-ray diffraction study. *Phys. Earth Planet. Inter.* **2017**, *265*, 82−91.

(13) Fernandez-Martinez, A.; Kalkan, B.; Clark, S. M.; Waychunas, G. A. Pressure-Induced Polyamorphism and Formation of "Aragonitic" Amorphous Calcium Carbonate. *Angew. Chem., Int. Ed.* **2013**, *52*, 8354−8357.

(14) Glasby, G. Abiogenic origin of hydrocarbons: An historical overview. *Resour. Geol.* **2006**, *56*, 85−98.

(15) Litasov, K. D.; Shatskiy, A.; Ohtani, E. Melting and subsolidus phase relations in peridotite and eclogite systems with reduced COH fluid at 3-16 GPa. *Earth Planet. Sci. Lett.* **2014**, *391*, 87−99.

(16) Shatskiy, A.; Borzdov, Y. M.; Litasov, K. D.; Kupriyanov, I. N.; Ohtani, E.; Palyanov, Y. N. Phase relations in the system FeCO3-CaCO3 at 6 GPa and 900-1700 °C and its relation to the system CaCO3-FeCO3-MgCO3. *Am. Mineral.* **2014**, *99*, 773−785.

(17) Podborodnikov, I. V.; Shatskiy, A.; Arefiev, A. V.; Rashchenko, S. V.; Chanyshev, A. D.; Litasov, K. D. The system Na_2CO_3−$CaCO_3$ at 3 GPa. *Phys. Chem. Miner.* **2018**, *45*, 773−787.

(18) Vennari, C. E.; Beavers, C. M.; Williams, Q. High-pressure/temperature behavior of the alkali/calcium carbonate shortite ($Na_2Ca_2(CO_3)_3$): Implications for carbon sequestration in Earth's transition zone. *J. Geophys. Res.: Solid Earth* **2018**, *123*, 6574−6591.

(19) Sverjensky, D. A.; Stagno, V.; Huang, F. Important role for organic carbon in subduction-zone fluids in the deep carbon cycle. *Nat. Geosci.* **2014**, *7*, 909−913.

(20) Sverjensky, D. A.; Huang, F. Diamond formation due to a pH drop during fluid-rock interactions. *Nat. Commun.* **2015**, *6*, 8702.

(21) Stanton, J. F.; Lopreore, C. L.; Gauss, J. The equilibrium structure and fundamental vibrational frequencies of dioxirane. *J. Chem. Phys.* **1998**, *108*, 7190−7196.

(22) Goryainov, S. V.; Krylov, A. S.; Polyansky, O. P.; Vtyurin, A. N. In-situ Raman study of phengite compressed in water medium under simultaneously high P-T parameters. *J. Raman Spectrosc.* **2017**, *48*, 1431−1437.

(23) Goryainov, S. V.; Krylov, A. S.; Vtyurin, A. N.; Pan, Y. Raman study of datolite $CaBSiO_4(OH)$ at simultaneously high pressure and high temperature. *J. Raman Spectrosc.* **2015**, *46*, 177−181.

(24) Rashchenko, S. V.; Likhacheva, A. Y.; Goryainov, S. V.; Krylov, A. S.; Litasov, K. D. In situ spectroscopic study of water intercalation into talc: New features of 10 Å phase formation. *Am. Mineral.* **2016**, *101*, 431−436.
(25) Goryainov, S. V.; Krylov, A. S.; Vtyurin, A. N.; Likhacheva, A. Y.; Prasad, P. S. R. In situ Raman study of wairakite and dawsonite interaction with water at high P-T parameters. *Bull. Russ. Acad. Sci.: Phys.* **2016**, *80*, 522−524.
(26) Datchi, F.; Dewaele, A.; Loubeyre, P.; Letoullec, R.; Le Godec, Y.; Canny, B. Optical pressure sensors for high-pressure−high-temperature studies in a diamond anvil cell. *High Pres. Res.* **2007**, *27*, 447−463.
(27) Krylov, A. S.; Gudim, I. A.; Nemtsev, I.; Krylova, S. N.; Shabanov, A. V.; Krylov, A. A. Raman study of $HoFe_3(BO_3)_4$ at simultaneously high pressure and high temperature: P−T phase diagram. *J. Raman Spectrosc.* **2017**, *48*, 1406−1410.
(28) Johannes, W.; Puhan, D. The calcite-aragonite transition, reinvestigated. *Contrib. Mineral. Petrol.* **1971**, *31*, 28−38.
(29) Borodina, U.; Likhacheva, A.; Golovin, A.; Goryainov, S.; Rashchenko, S.; Korsakov, A. Raman spectra of shortite $Na_2Ca_2(CO3)_3$ compressed up to 8 GPa. *High Pres. Res.* **2018**, *38*, 293−302.
(30) *Model S506 Interactive Peak Fit. User's Manual*; Canberra Industries, Inc.: United States of America, 2002.
(31) Goryainov, S. V.; Smirnov, M. B. Raman spectra and lattice-dynamical calculations of natrolite. *Eur. J. Mineral.* **2001**, *13*, 507−519.
(32) Goryainov, S. V.; Pan, Y.; Smirnov, M. B.; Sun, W.; Mi, J.-X. Raman investigation on the behavior of parasibirskite $CaHBO_3$ at high pressure. *Spectrochim. Acta, Part A* **2017**, *173*, 46−52.
(33) Goryainov, S. V. Raman study of thaumasite $Ca_3Si(OH)_6(SO_4)(CO_3)_12H_2O$ at high pressure. *J. Raman Spectrosc.* **2016**, *47*, 984−992.
(34) Clark, S. J.; Pickard, C. J.; Hasnip, P. J.; Refson, K.; Payne, M. C.; Refson, K.; Payne, M. First principles methods using CASTEP. *Z. Kristallogr.-Cryst. Mater.* **2005**, *220*, 567−570.
(35) Monkhorst, H. J.; Pack, J. D. Special points for Brillouin-zone integrations. *Phys. Rev. B: Condens. Matter Mater. Phys.* **1976**, *13*, 5188−5192.
(36) Perdew, J. P.; Ruzsinszky, A.; Csonka, G. I.; Vydrov, O. A.; Scuseria, G. E.; Constantin, L. A.; Zhou, X.; Burke, K. Restoring the Density-Gradient Expansion for Exchange in Solids and Surfaces. *Phys. Rev. Lett.* **2008**, *100*, 136406.
(37) Rashchenko, S. V.; Goryainov, S. V.; Romanenko, A. V.; Golovin, A. V.; Korsakov, A. V.; Moine, B. N.; Mikhno, A. O. High-pressure Raman study of nyerereite from Oldoinyo Lengai. *J. Raman Spectrosc.* **2017**, *48*, 1438−1442.
(38) Frost, R. L.; Dickfos, M. J. Raman and infrared spectroscopic study of the anhydrous carbonate minerals shortite and barytocalcite. *Spectrochim. Acta, Part A* **2008**, *71*, 143−146.
(39) Spycher, N.; Pruess, K.; Ennis-King, J. CO_2-H_2O mixtures in the geological sequestration of CO_2. I. Assessment and calculation of mutual solubilities from 12 to 100 C and up to 600 bar. *Geochim. Cosmochim. Acta* **2003**, *67*, 3015−3031.
(40) SDBS. SDBS Web: http://sdbs.db.aist.go.jp; National Institute of Advanced Industrial Science and Technology, 31, 03, 1999 (SDBS No.: 2964).
(41) Tajima, I.; Takahashi, H.; Machida, K. Polarized i.r. reflection and Raman spectra of sodium formate crystal. *Spectrochim. Acta, Part A* **1981**, *37*, 905−910.
(42) Heyns, A. M. The effect of pressure on the Raman spectra of solids. III. Sodium formate, NaHCOO. *J. Chem. Phys.* **1986**, *84*, 3610.
(43) Wang, S.; Kong, P.; Zhang, Z.; Sun, H.; Li, P.; Chen, R.; Gu, B.; Ungar, G.; Wu, X.; Cheng, L.; et al. Structure, morphology, and nonlinear optical properties of orthorhombic alfa-$Ca(HCOO)_2$ single crystals. *Opt. Mater. Express* **2018**, *8*, 2238−2245.
(44) Spinner, E. Vibration-spectral studies of carboxylate ions. Part III. Sodium formate, HCO_2Na and DCO_2Na; Raman-spectral depolarisation ratios in aqueous solution, and band splitting in the solid-state infrared spectrum. *J. Chem. Soc. B* **1967**, *0*, 879−885.
(45) Noma, H.; Machida, K. Polarized Raman intensities of sodium formate crystal and its non-cylindrical electrooptical parameters. *J. Mol. Struct.* **1990**, *224*, 163−174.
(46) Hoffmann, F. M.; Yang, Y.; Paul, J.; White, M. G.; Hrbek, J. Hydrogenation of carbon dioxide by water: Alkali-promoted synthesis of formate. *J. Phys. Chem. Lett.* **2010**, *1*, 2130−2134.
(47) Sobolev, N. V.; Tomilenko, A. A.; Bul'bak, T. A.; Logvinova, A. M. Composition of Hydrocarbons in Diamonds, Garnet, and Olivine from Diamondiferous Peridotites from the Udachnaya Pipe in Yakutia, Russia. *Engineering* **2019**, *5*, 471−478.

https://doi.org/10.1021/acs.jpcc.1c05077
J. Phys. Chem. C 2021, 125, 18501−18509